ON THE INVERSION OF THE ANSCOMBE TRANSFORMATION IN LOW-COUNT POISSON IMAGE DENOISING

Markku Mäkitalo and Alessandro Foi

Department of Signal Processing, Tampere University of Technology
P.O. Box 553, 33101, Tampere, Finland
web: http://www.cs.tut.fi/~foi email: firstname.lastname@tut.fi

ABSTRACT

The removal of Poisson noise is often performed through the following three-step procedure. First, the noise variance is stabilized by applying the Anscombe root transformation to the data, producing a signal in which the noise can be treated as additive Gaussian noise with unitary variance. Second, the noise is removed using a conventional denoising algorithm for additive white Gaussian noise. Third, an inverse transformation is applied to the denoised signal, obtaining the estimate of the signal of interest.

The choice of the proper inverse transformation is crucial in order to minimize the bias error which arises when the nonlinear forward transformation is applied. We present an experimental analysis using a few state-of-the-art denoising algorithms and show that the estimation can be consistently improved by applying the exact unbiased inverse, particularly at the low-count regime.

1. INTRODUCTION

Poisson noise is characteristic of many image acquisition modalities. Its removal is of fundamental importance for many applications and particularly in astronomy and medical imaging. Although denoising algorithms specifically designed for Poisson noise have been proposed, often the removal of Poisson noise is performed through the following three-step procedure. First, the noise variance is stabilized by applying the Anscombe root transformation [1] $f : z \longmapsto 2\sqrt{z+\frac{3}{8}}$ to the data. This produces a signal in which the noise can be treated as additive Gaussian noise with unitary variance. Second, the noise is removed using a conventional denoising algorithm for additive white Gaussian noise. Third, an inverse transformation is applied to the denoised signal, obtaining the estimate of the signal of interest.

This paper focuses on this last step and aims at identifying and emphasizing the role that the inversion plays in ensuring the success of the whole procedure.

In the recent years, variance stabilization has often been questioned as a viable method for Poisson noise removal because of the poor numerical results achieved at the low-count regime, i.e. for low-intensity signals. We show that this disappointing performance, showed in many earlier works (e.g. [8], [6]), is not due to the stabilization itself (i.e. to the forward transformation), but rather to the inverse transformation.

The choice of the proper inverse transformation is crucial in order to minimize the bias error which arises when the nonlinear forward transformation is applied. Both the algebraic inverse and the asymptotically unbiased inverse proposed by Anscombe [1] lead to a significant bias at low counts. In particular, the latter inverse provides unbiasedness only asymptotically for large counts while at low counts it leads to a larger bias than the former one.

We present an experimental analysis using a few state-of-the-art denoising algorithms and show that the results can be consistently improved by applying the exact unbiased inverse. In particular, the combination of BM3D [3] and the exact unbiased inverse outperforms some of the best existing algorithms specifically targeted at Poisson noise removal.

2. PRELIMINARIES

2.1 Poisson noise

Let $z_i, i = 1, \ldots, N$ be the observed pixel values obtained through an image acquisition device. We consider each z_i to be an independent random Poisson variable whose mean y_i is the underlying intensity value to be estimated. In addition to being the mean of the Poisson variable z_i, the parameter y_i is also its variance:

$$E\{z_i \mid y_i\} = y_i = \text{var}\{z_i \mid y_i\}. \tag{1}$$

Poisson noise can be formally defined as

$$\eta_i = z_i - E\{z_i \mid y_i\}, \tag{2}$$

thus, we trivially have $E\{\eta_i \mid y_i\} = 0$ and $\text{var}\{\eta_i \mid y_i\} = \text{var}\{z_i \mid y_i\} = y_i$.

2.2 Variance stabilization and the Anscombe transformation

The rationale behind applying a variance-stabilizing transformation is to remove the data-dependence of the noise variance, so that it becomes constant throughout the whole data $z_i, i = 1, \ldots, N$. Moreover, if the transformation is also normalizing (i.e. it results in a Gaussian noise distribution), we

This work was supported by the Academy of Finland (project no. 213462, Finnish Programme for Centres of Excellence in Research 2006-2011, project no. 118312, Finland Distinguished Professor Programme 2007-2010, and project no. 129118, Postdoctoral Researcher's Project 2009-2011).

978-1-4244-5167-8/09/$25.00 ©2009 IEEE

can estimate the intensity values y_i with a conventional denoising method designed for additive white Gaussian noise. Neither exact stabilization nor exact normalization are possible ([4], [5]), therefore, in practice, approximate solutions are employed.

One of the most popular variance-stabilizing transformations is the Anscombe transformation [1]

$$f(z) = 2\sqrt{z + \frac{3}{8}}. \tag{3}$$

Applying (3) to Poisson distributed data gives a signal whose noise is asymptotically additive standard normal.

The denoising of $f(z)$ produces a signal D that can be considered as an estimate of $E\{f(z) \mid y\}$. We need to apply an inverse transformation to D in order to obtain the wanted estimate of y. The direct algebraic inverse of (3) is

$$\mathcal{I}_A(D) = f^{-1}(D) = \left(\frac{D}{2}\right)^2 - \frac{3}{8}, \tag{4}$$

but the resulting estimate of y is biased, because the nonlinearity of the transformation f means we generally have

$$E\{f(z) \mid y\} \neq f(E\{z \mid y\}), \tag{5}$$

and, thus,

$$f^{-1}(E\{f(z) \mid y\}) \neq E\{z \mid y\}. \tag{6}$$

Another possibility is to use the adjusted inverse [1]

$$\mathcal{I}_B(D) = \left(\frac{D}{2}\right)^2 - \frac{1}{8}, \tag{7}$$

which provides asymptotical unbiasedness for large counts. This is the inverse typically used in applications.

2.3 Exact unbiased inverse

While the asymptotically unbiased inverse (7) provides good results for high-count data, applying it to low-count data leads to a biased estimate, as can be seen e.g. in [8]. Provided a successful denoising (i.e. D is treated as $E\{f(z) \mid y\}$), the key to solving this problem is to find the exact unbiased inverse of the Anscombe transformation f, i.e. to find an inverse transformation $\mathcal{I}_C$ that maps the values $E\{f(z) \mid y\}$ to the desired values $E\{z \mid y\}$:

$$\mathcal{I}_C : E\{f(z) \mid y\} \longmapsto E\{z \mid y\}. \tag{8}$$

Since, for any given y, $E\{z \mid y\} = y$, the problem of finding the inverse $\mathcal{I}_C$ reduces to computing the values $E\{f(z) \mid y\}$, which is done by numerical evaluation of the integral corresponding to the expectation operator E:

$$E\{f(z) \mid y\} = \int_{-\infty}^{+\infty} f(z)\, p(z \mid y)\, dz, \tag{9}$$

where $p(z \mid y)$ is the generalized probability density function of z conditioned on y. In our case we have discrete Poisson probabilities $P(z \mid y)$, so we can replace the integral by summation:

$$E\{f(z) \mid y\} = \sum_{z=0}^{+\infty} f(z) P(z \mid y). \tag{10}$$

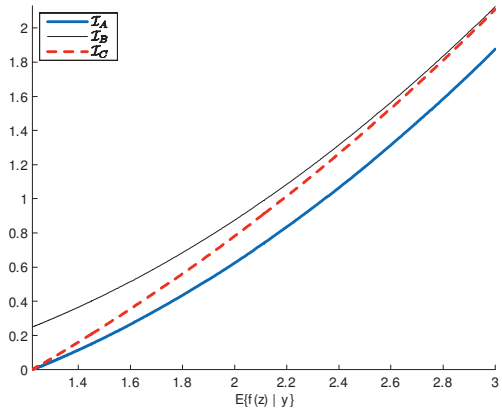

Figure 1: Inverse transformations $\mathcal{I}_A$ (algebraic), $\mathcal{I}_B$ (asymptotically unbiased) and $\mathcal{I}_C$ (exact unbiased).

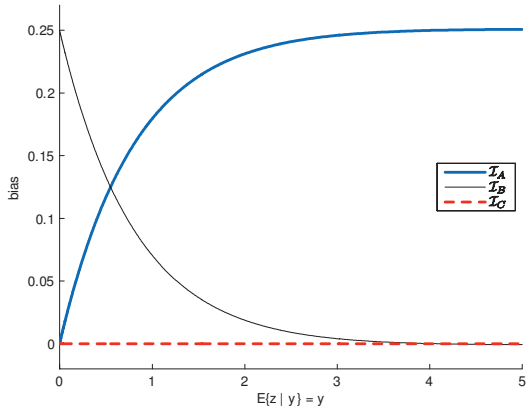

Figure 2: Absolute value of the bias of the inverse transformations $\mathcal{I}_A$, $\mathcal{I}_B$ and $\mathcal{I}_C$.

Further, since here $f(z)$ is the forward Anscombe transformation (3), we can write Eq. (10) as

$$E\{f(z) \mid y\} = 2\sum_{z=0}^{+\infty}\left(\sqrt{z + \frac{3}{8}} \cdot \frac{y^z e^{-y}}{z!}\right). \tag{11}$$

In practice, it is sufficient to compute (11) for a limited set of values y: for arbitrary values of y we use linear interpolation based on these computed values of (11), and for large values of y we approximate $\mathcal{I}_C$ by $\mathcal{I}_B$.

A Matlab function implementing the exact unbiased inverse transformation $\mathcal{I}_C$ is available online at http://www.cs.tut.fi/~foi/invansc.

Figure 1 shows the plots of the inverse transformations $\mathcal{I}_A$, $\mathcal{I}_B$ and $\mathcal{I}_C$. We see that at low counts the asymptotically unbiased inverse actually leads to a larger bias than the algebraic inverse; this is also explicitly illustrated in Figure 2.

3. EXPERIMENTS

Our experiments are done in the same way as in [8] in order to produce comparable results; the authors of [8] also kindly provided us with their set of test images (all of them 256x256 in size). The same simulation scenario was used also in [6].

We proceed as follows: First we apply the forward Anscombe transformation (3) to a noisy image. Then we denoise the transformed image (assuming additive white Gaussian noise of unit variance) with either BM3D [3], SAFIR [2] or BLS-GSM [7], and finally we apply the exact unbiased inverse in order to get the final estimate. We evaluate the performance by using normalized mean integrated square error (NMISE), which is calculated using the formula

$$\frac{1}{\bar{N}} \sum_{i:y_i>0} \left((\hat{y}_i - y_i)^2 / y_i \right), \tag{12}$$

where $\hat{y}_i$ are the estimated intensities, y_i the respective true values, and the sum is computed over the $\bar{N}$ pixels in the image for which $y_i > 0$. For each image this procedure is performed five times, each time with a different realization of the random noise. The obtained NMISE values are finally averaged over these five replications.

The same experiments are also done for the asymptotically unbiased inverse (7), whose results serve as a point of comparison.

The numerical results of our experiments are presented in Table 1, where we also compare them to the results obtained with the PH-HMT and MS-VST algorithms proposed in [6] and [8], respectively. Both of these algorithms are specifically targeted at Poisson noise removal, and both of them have produced state-of-the-art results. In addition, we have included the results obtained in [8] with the asymptotically unbiased inverse Anscombe transformation combined with various undecimated wavelet transforms (here collectively denoted as WT). Table 1 shows not only that the exact unbiased inverse produces significantly better results at low counts than the asymptotically unbiased inverse, but also that the method is competitive with both PH-HMT and MS-VST. In particular, the combination of BM3D and the exact unbiased inverse outperforms both of them in terms of NMISE.

Figures 3-7 illustrate the improvement that is achieved (especially at low counts) by applying the exact unbiased inverse instead of the asymptotically unbiased inverse, while Figures 8-10 compare the different algorithms for the denoising of the Ridges, Barbara and Cells images (the exact unbiased inverse combined with BM3D, SAFIR and BLS-GSM, and the best MS-VST result from [8]). In addition, we present a chosen cross-section (i.e. one row) of each test image in Figure 11. These plots also clearly demonstrate that at low counts the exact unbiased inverse provides a significant improvement over the asymptotically unbiased inverse, while at high counts the difference is expectedly negligible.

4. DISCUSSION AND CONCLUSIONS

In this paper we showed that the three-step procedure of first stabilizing the noise variance by applying the Anscombe transformation, then denoising with an algorithm designed for Gaussian noise, and finally applying an inverse transformation, can still be considered a viable approach for Poisson noise removal. In particular, the poor performance of the asymptotically unbiased inverse at low counts can be overcome by replacing it with the exact unbiased inverse. Further, when combined with a state-of-the-art Gaussian denoising algorithm, this method is competitive with some of the best Poisson noise removal algorithms, such as PH-HMT [6] and MS-VST [8]. While most of the improvement is due to the exact unbiased inverse, the choice of the denoising algorithm does also matter, and in particular BM3D consistently outperforms the other methods considered here.

In this paper we contemplated only imaging, but it is worth noting that the same procedure can be applied to data of any dimension, including 1-D signals and volumetric data.

5. ACKNOWLEDGMENT

We would like to thank Bo Zhang and Jalal Fadili for providing us with the images used in our experiments, and Charles Kervrann and Jérôme Boulanger for providing us with their denoising software (SAFIR) and suitable parameters for it.

REFERENCES

[1] Anscombe, F.J., "The transformation of Poisson, binomial and negative-binomial data", *Biometrika*, vol. 35, no. 3/4, pp. 246–254, Dec. 1948.

[2] Boulanger, J., J.B. Sibarita, C. Kervrann, and P. Bouthemy, "Non-parametric regression for patch-based fluorescence microscopy image sequence denoising", *Proc. IEEE Int. Symp. on Biomedical Imaging (ISBI'08)*, pp. 748–751, May 2008.

[3] Dabov, K., A. Foi, V. Katkovnik, and K. Egiazarian, "Image denoising by sparse 3D transform-domain collaborative filtering", *IEEE Trans. Image Process.*, vol. 16, no. 8, pp. 2080–2095, Aug. 2007.

[4] Curtiss, J.H., "On transformations used in the analysis of variance", *The Annals of Mathematical Statistics*, vol. 14, no. 2, pp. 107–122, June 1943.

[5] Efron, B., "Transformation theory: How normal is a family of distributions?", *The Annals of Statistics*, vol. 10, no. 2, pp. 323–339, 1982.

[6] Lefkimmiatis, S., P. Maragos, and G. Papandreou, "Bayesian inference on multiscale models for Poisson intensity estimation: Applications to photon-limited image denoising", *IEEE Trans. Image Process.*, vol. 18, no. 8, pp. 1724–1741, Aug. 2009.

[7] Portilla, J., V. Strela, M.J. Wainwright, and E.P. Simoncelli, "Image denoising using scale mixtures of Gaussians in the wavelet domain", *IEEE Trans. Image Process.*, vol. 12, no. 11, pp. 1338–1351, Nov. 2003.

[8] Zhang B., J.M. Fadili, and J-L. Starck, "Wavelets, ridgelets, and curvelets for Poisson noise removal", *IEEE Trans. Image Process.*, vol. 17, no. 7, pp. 1093–1108, July 2008.

	Asymptotically unbiased inverse				Exact unbiased inverse			Other algorithms	
	WT [8]	BM3D	SAFIR	BLS-GSM	BM3D	SAFIR	BLS-GSM	PH-HMT [6]	MS-VST [8]
Spots [0.03, 5.02]	2.34	1.7395	1.7495	2.0370	**0.0365**	0.0384	0.2024	0.048	0.069
Galaxy [0, 5]	0.15	0.1025	0.1110	0.1253	**0.0299**	0.0301	0.0385	0.030	0.035
Ridges [0.05, 0.85]	0.83	0.7018	0.7252	0.7694	**0.0128**	0.0173	0.0332	-	0.017
Barbara [0.93, 15.73]	0.26	0.0880	0.1178	0.1122	**0.0880**	0.1178	0.1123	0.159	0.17
Cells [0.53, 16.93]	0.095	0.0660	0.0683	0.0718	**0.0649**	0.0671	0.0707	0.082	0.078

Table 1: Average NMISE values for the asymptotically unbiased inverse and the exact unbiased inverse, and a comparison to the results obtained in [6] and [8] with algorithms specifically designed for Poisson noise removal. The intensity range of each image is indicated in brackets.

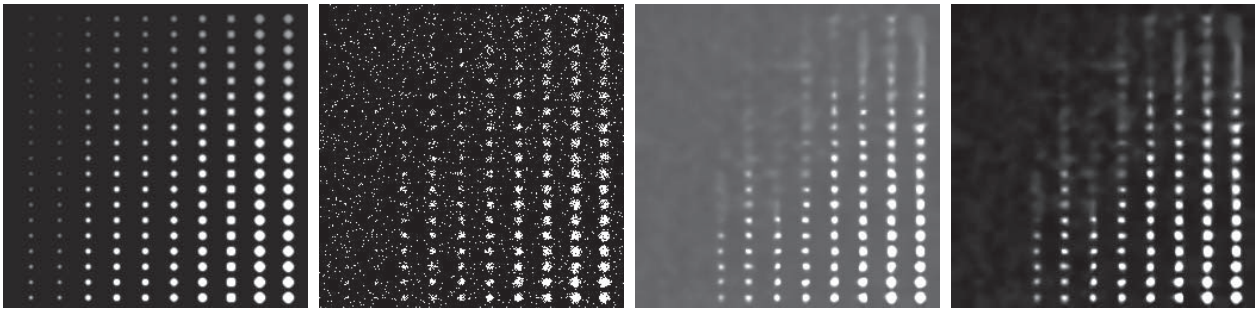

(a) (b) (c) (d)

Figure 3: (a) Original Spots image (intensity range [0.03, 5.02]), (b) Poisson-count image, (c) image denoised with BM3D and the asymptotically unbiased inverse (average NMISE = 1.7395), (d) image denoised with BM3D and the exact unbiased inverse (average NMISE = 0.0365).

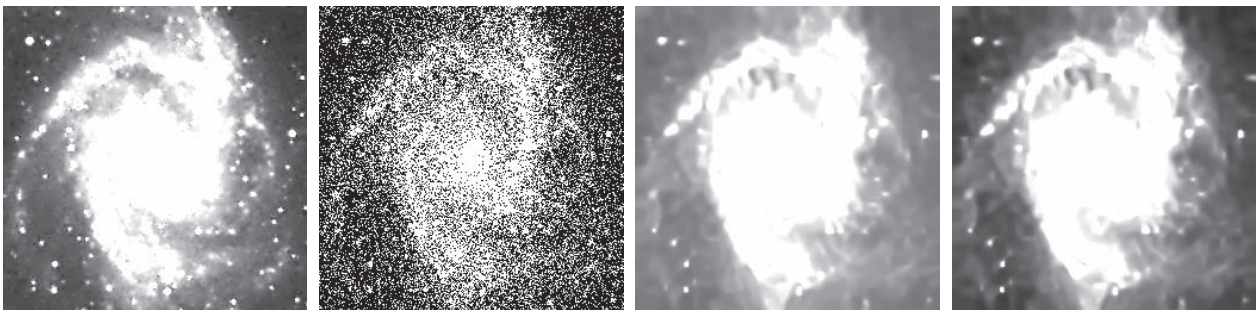

(a) (b) (c) (d)

Figure 4: (a) Original Galaxy image (intensity range [0, 5]), (b) Poisson-count image, (c) image denoised with BM3D and the asymptotically unbiased inverse (average NMISE = 0.1025), (d) image denoised with BM3D and the exact unbiased inverse (average NMISE = 0.0299).

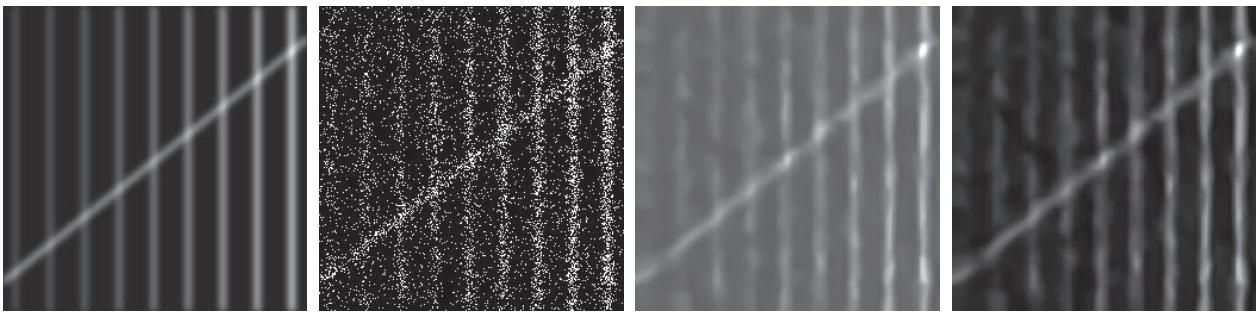

(a) (b) (c) (d)

Figure 5: (a) Original Ridges image (intensity range [0.05, 0.85]), (b) Poisson-count image, (c) image denoised with BM3D and the asymptotically unbiased inverse (average NMISE = 0.7018), (d) image denoised with BM3D and the exact unbiased inverse (average NMISE = 0.0128).

(a) (b) (c) (d)

Figure 6: (a) Original Barbara image (intensity range [0.93, 15.73]), (b) Poisson-count image, (c) image denoised with BM3D and the asymptotically unbiased inverse (average NMISE = 0.0880), (d) image denoised with BM3D and the exact unbiased inverse (average NMISE = 0.0880).

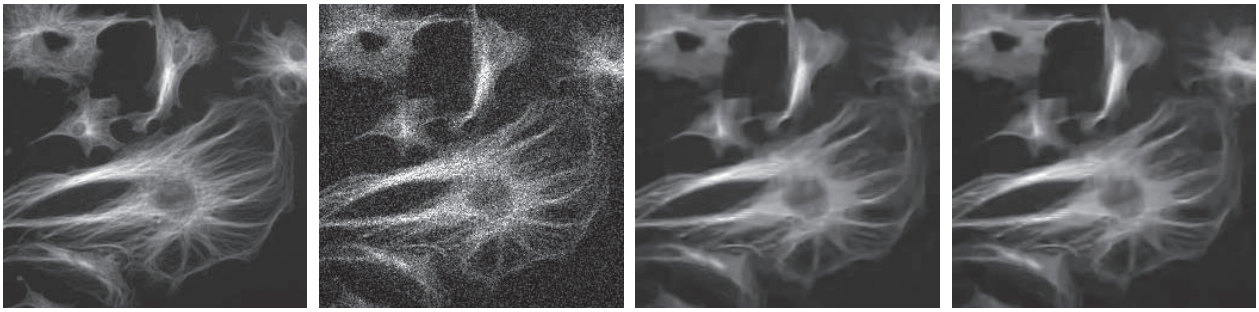

(a) (b) (c) (d)

Figure 7: (a) Original Cells image (intensity range [0.53, 16.93]), (b) Poisson-count image, (c) image denoised with BM3D and the asymptotically unbiased inverse (average NMISE = 0.0660), (d) image denoised with BM3D and the exact unbiased inverse (average NMISE = 0.0649).

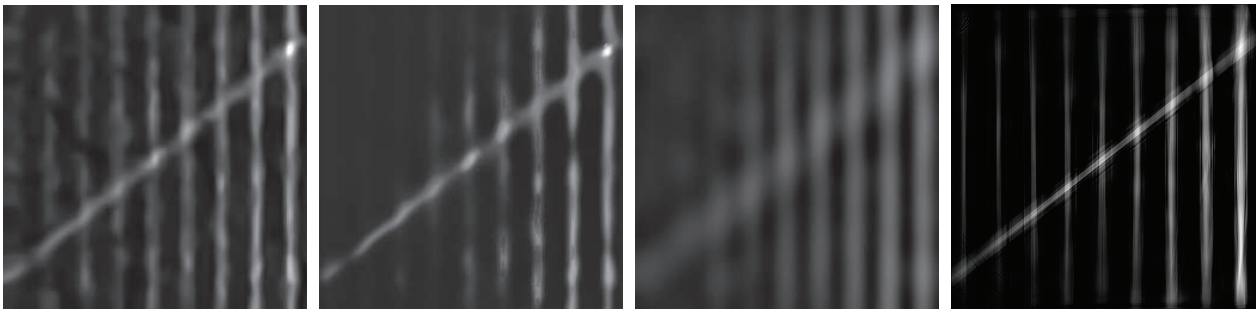

(a) (b) (c) (d)

Figure 8: Ridges denoised with (a) BM3D and the exact unbiased inverse (average NMISE = 0.0128), (b) SAFIR and the exact unbiased inverse (average NMISE = 0.0173), (c) BLS-GSM and the exact unbiased inverse (average NMISE = 0.0332), (d) MS-VST + ridgelets (average NMISE = 0.017) [8]. The original and noisy images are shown in Figure 5.

(a) (b) (c) (d)

Figure 9: Barbara denoised with (a) BM3D and the exact unbiased inverse (average NMISE = 0.0880), (b) SAFIR and the exact unbiased inverse (average NMISE = 0.1178), (c) BLS-GSM and the exact unbiased inverse (average NMISE = 0.1123), (d) MS-VST + curvelets (average NMISE = 0.17) [8]. The original and noisy images are shown in Figure 6.

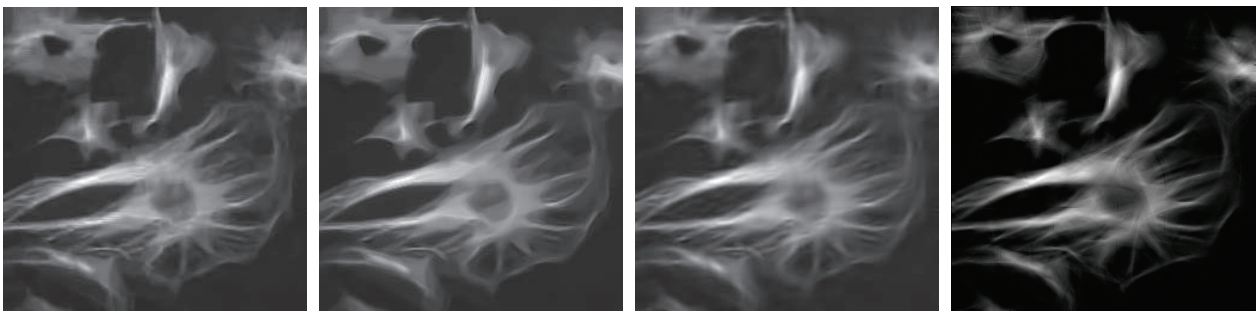

(a) (b) (c) (d)

Figure 10: Cells denoised with (a) BM3D and the exact unbiased inverse (average NMISE = 0.0649), (b) SAFIR and the exact unbiased inverse (average NMISE = 0.0671), (c) BLS-GSM and the exact unbiased inverse (average NMISE = 0.0707), (d) MS-VST + curvelets (average NMISE = 0.078) [8]. The original and noisy images are shown in Figure 7.

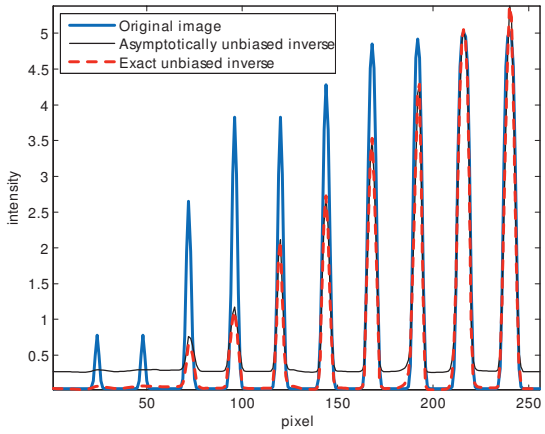

(a) Spots (row 247).

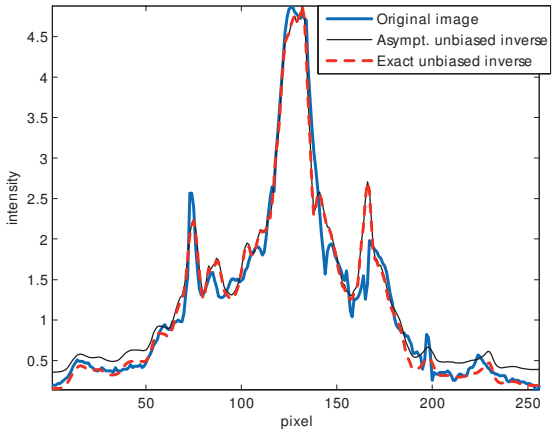

(b) Galaxy (row 130).

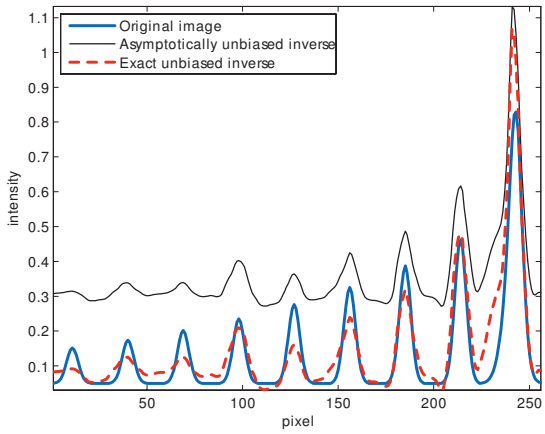

(c) Ridges (row 40).

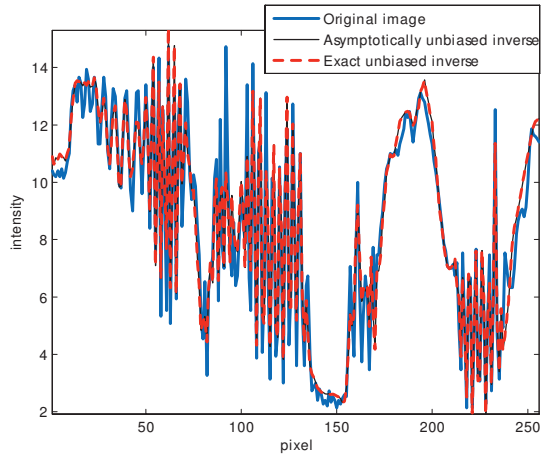

(d) Barbara (row 200).

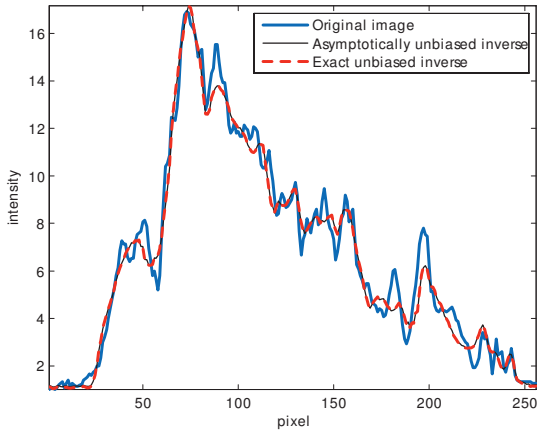

(e) Cells (row 145).

Figure 11: Cross-sections of the images denoised with BM3D. For Barbara and Cells the intensities are large enough for the two inverses to practically coincide.